JOM, 65 (2013) 870-882
http://dx.doi.org/10.1007/s11837-013-0616-1

Metastable soft magnetic materials produced by mechanical alloying: Analysis using an equivalent time approach

J. S. Blázquez[1], J. J. Ipus[1], S. Lozano-Pérez[2], A. Conde[1]

1.-Dpto. Física de la Materia Condensada, ICMSE-CSIC, Universidad de Sevilla, P.O. Box 1065, 41080, Sevilla, Spain.

2.-Department of Materials, University of Oxford, Parks Road, Oxford OX1 P3H, UK.

Corresponding author: J. S. Blázquez

E-mail: jsebas@us.es

Tel: +34 954 55 60 29

Fax: +34 954 61 20 97

Abstract

Mechanical alloying, a ball milling technique where heterogeneous starting powders are homogenized and alloyed, has become a versatile technique for the production of metastable microstructures: nanocrystalline and/or amorphous alloys, supersaturated solid solutions, etc. Ball milling is affected by many experimental parameters and the analysis of the dynamics of milling is needed in order to compare different experiments and to optimize time and costs. In this work, a short overview on the microstructural techniques used to characterize the powder is supplied. The soft magnetic properties of mechanically alloyed powders are also described, as well as the magnetocaloric response of these systems.

Keywords: Mechanical alloying; soft magnetic alloys.

JOM, 65 (2013) 870-882
http://dx.doi.org/10.1007/s11837-013-0616-1

1. Introduction

Ball milling experienced an inflexion point after Benjamin used it to disperse oxide particles in Ni-based alloys. The experiments performed at the International Nickel Company (INCO) gave birth to the mechanical alloying (MA) method [1]. MA must be distinguished from mechanical grinding and mechanical disordering as described by Suryanarayana [2]. In these two other ball milling techniques, the starting material has a homogeneous composition and thus no net material transfer may occur. Mechanical disordering may even yield the destruction of long range order in the starting material producing amorphous systems. For MA processes, however, the starting material is not homogeneous but, generally, a mixture of commercial pure powders and/or intermetallic compounds. During MA, material transfer occurs and the heterogeneous starting material increases homogenization as a first step of the process.

In order to show the scientific interest on MA, searches using Web of Science database have been performed. The number of scientific papers published on this subject were estimated searching “ball mill*” OR “mechanical alloy*” in the topic field obtaining a number of papers N_{MA} (growing from 1 to 1420 from 1965 to 2012). A control search to take into account the general increase in publications was also done using “material*” as topic, N_{Total}. The relative number of papers published was estimated as the ratio N_{MA}/N_{Total} normalized to its value in 1965. Figure 1 shows these estimated relative number of papers published between 1965 and 2012. After Benjamin’s discovery, an important milestone was the development of amorphous alloys in the 80s [3, 4], which had a marked effect on the interest devoted to MA. Contemporary to this, a rise in the interest of the scientific community on amorphous and nanocrystalline systems occurs due to their outstanding magnetic [5] and mechanical properties [6]. The plateau observed in Fig. 1 since then to the present day

occurs even though, as long as MA had become a conventional technique to produce metastable phases, the name of the technique may not appear in the topic field.

Most of the laboratory MA studies are performed using a planetary mill with a maximum load limited to a few tens of grams of powder or a shaker mill (Spex), limited to 10 g of load. However, loads of attritor mills can exceed 100 kg, so the route to extend the laboratory results to industrial production is straightforward. In this sense, the knowledge of the different power released from the milling media to the powder is an important task in order to reproduce the same results using different mill conditions. In planetary mills, the movement resembles that of pairs of orbiting planets around the center of a main disc and rotating around its own axis. Vials in Spex mills describe a more complex movement similar to a figure of eight.

Besides the type of mill, the energy transferred to the powder is affected by a numerous set of parameters. Among the most important are: milling time, frequency, number and size of balls as well as material used as milling media (which also affects the contamination). In order to compare different milling experiments, it is assumed that the degree of evolution of a milled powder is only dependent on the amount of energy transferred to it. This approximation is not fulfilled when the explored parameter or property is very sensitive to temperature, as temperature in the vial during milling is also dependent on milling parameters as it will be shown below.

The aim of the present paper is to give a short overview on the soft magnetic materials produced by ball milling. It is structured in five sections, including this introduction.

In the second section, the dynamics of a planetary ball mill are analyzed. The power transferred from the milling media to the powder is shown to be proportional to

the cube of the frequency of the disc, which leads to the definition of an equivalent milling time enabling comparisons between different milling experiments performed under different conditions.

In the third section, the microstructure evolution of Fe-based systems as milling progresses is described. The two scale character of the resulting powder samples is highlighted: powder particle size and crystal (or grain) size. Scanning electron microscopy (SEM) successfully characterizes the particle size, whereas X-ray diffraction (XRD) is widely used to estimate crystal size. Special attention is focused on the difficulty of sample preparation for transmission electron microscopy (TEM), especially for magnetic powders. Some examples on analytical techniques such as energy dispersive spectroscopy (EDS) and energy filtered TEM (EFTEM) images will be shown.

The fourth section is devoted to magnetic properties of soft-magnetic Fe-based amorphous and nanocrystalline alloys obtained by ball milling including magnetocaloric effect and Mössbauer spectroscopy.

Finally, some comments on the thermal stability of the powder obtained appear in the fifth section.

2. Dynamics of planetary ball mills: equivalent time approximation

Delogu et al.[7], studying the behavior of Spex mills, defined the dose as the amount of energy transferred during milling and this concept can be extended to other types of mills. For further information on the dynamics of Spex mills, the following references are suggested to the reader [7],[8-10].

JOM, 65 (2013) 870-882
http://dx.doi.org/10.1007/s11837-013-0616-1

Following the model of Abdellaui and Gaffet [11], we studied the dynamics of the planetary mills using a simple model [12] that considers a two dimensional movement of a single ball into the vial. This ball moves under the action of two forces, both exerted by the vial wall: normal and friction forces, N and F_μ, respectively.

$$N = m\left[\omega^2 r + \Omega^2 R\cos\left(\left(\omega+\Omega\right)t+\varphi_0\right)\right]$$

$$F_\mu = m\left[\Omega^2 R\sin\left(\left(\omega+\Omega\right)t+\varphi_0\right)\right]$$

where m is the mass of the ball, ω and Ω are the rotational frequencies of the vial and the disc, respectively, r and R are the radii of the vial and the disc, respectively, t is the time and φ_0 should indicate the position of the ball at the t=0.

As long as N>0, the ball moves attached to the vial wall. Once N=0, the ball detaches and starts a free movement till it collides with the vial wall again. After colliding, we assume a complete inelastic collision and ball keeps moving attached to the vial wall. Figures 2(b) and (d) show the trajectories inside the vial followed by a single ball in P5 (see Fig. 2(a)) and P4 vario (see Fig. 2(c)) Fritsch Pulverisette planetary mills. Whereas ω/Ω is fixed for P5, this magnitude can be changed in P4 mill. The trajectories shown corresponds to the parameters of the example experiments used in this work, where ω/Ω=-2 independently of the mill. From the calculated trajectories it is inferred that the approximation of completely inelastic collision should be better fulfilled in P4 mill than in P5.

The energy released to the powder mainly occurs when some powder is trapped between the ball and the vial wall during the impact (including as free powder as well as the powder coating balls and walls). The energy released is proportional to the kinetic energy and thus to Ω^2 each time the ball collides with the vial wall (friction maintains

JOM, 65 (2013) 870-882
http://dx.doi.org/10.1007/s11837-013-0616-1

this Ω^2 dependence). Moreover, as the evolution of the normal force indicates, the number of events occurring during one period time for a constant ω/Ω ratio is independent of the frequency value (without changing the geometry, i.e. the mill). Therefore, the power released should be equal to the number of collisions per unit time multiplied by the energy released in each collision, $E=k\Omega^2$.

$$P = \frac{N}{T} k\Omega^2 = k'\Omega^3$$

where N is the constant number of collisions per period T, thus a cubic law is inferred for the power released during milling.

An equivalent time is defined straightforward for the comparison of milling experiments performed at different frequencies in the same mill and maintaining the frequency ratio. This equivalent time must be referred to a reference frequency, Ω_0, as:

$$t_{eq} = \left(\frac{\Omega^3}{\Omega_0^{\ 3}} \right) t$$

In the examples supplied throughout this paper, taken from experiments performed in P4 or P5 Fritsch Pulverisette mills (see figure 2), results will be given as a function of the equivalent time with Ω_0=150 rpm. Since the total inelastic collision is better fulfilled in P4, rescaling using the equivalent times is also better fulfilled for the experiments performed in this mill than in P5[12, 13].

In order to test the equivalent time approach, the temperature increase inside the vial during milling was measured, ΔT. The temperature in the vial will increase due to the heat supplied during collisions and friction and thus will be proportional to the power release to the powder. The vial will lose heat to the environment through

JOM, 65 (2013) 870-882
http://dx.doi.org/10.1007/s11837-013-0616-1

conduction, being proportional to ΔT, and finally a stationary regime will be established in which the heat losses equal the heat released during milling:

$$\left.\frac{dQ_{Total}}{dt}\right|_{eq} = A\Omega^3 - B\Delta T = 0$$

$$\Delta T = k''\Omega^3$$

where A, B and $k''=A/B$ are constants depending on the different parameters involved in milling. Figure 2(e) shows the linear increase of saturation temperature in the vial (measured using a GTMII system) as a function of Ω^3. The temperature increase is quite low if only 50 steel balls in 250 cm^3 vial are used. When the number of balls increases to 75, an increase of the temperature at the outside wall of the vial ΔT=25 K for Ω=350 rpm has been found [14]. Estimation of the local temperature rise during the impact also yields relative low values (~100-200 ºC) [15, 16].

3. Evolution of microstructure

There are two scales present in powder samples: a micrometric length, which characterizes the size of the powder particles (in some cases they can join forming larger agglomerates), and a nanometric length characterizing the size of coherent diffraction regions, which can be associated to crystallites. Therefore, it is very important to avoid an ambiguous use of the terms particle and grain (or crystal). In order to do so, in the present paper powder particle and crystallite will be used. Only in some specific cases, using appropriate surfactants, nanopowder particles can be achieved, an especially interesting fact in the case of hard magnetic materials [17-20]. The use of cryomilling also helps in reducing the size of the powder particles, as cold

JOM, 65 (2013) 870-882
http://dx.doi.org/10.1007/s11837-013-0616-1

welding diminishes as temperature is reduced, and in retaining metastable phases by preventing recrystallization [21-23].

3.1 Powder particles characterization

In order to obtain information concerning the morphology, size and compositional distribution of powder particles, scanning electron microscopy (SEM) is a widely used technique. Samples for SEM observation are generally prepared by depositing some powder onto a carbon film. This does not supply the polished surfaces needed for some of the techniques available in modern SEMs (e.g. EBSD) but, on the other hand, samples are not affected by preparation. Two conventional SEM imaging modes are of interest: secondary electron mode (SE) and backscattered electron mode (BSE). Moreover, SEMs are generally equipped with analytical facilities (e. g. energy dispersive spectroscopy, EDS). SE mode is helpful to study the morphology and size distribution of the powder particles, whereas BSE mode supplies elemental contrast (back scattered electrons increase with the atomic mass of the target), which makes it especially interesting at the beginning of milling, when the elements are not intimately mixed (or alloyed). Figure 3(a-b) shows examples of SE and BSE images on a powder particle of a Fe-Nb-B composition at an early stage of milling process; very light boron particles appear as black regions. Figure 3(c) shows EDS spectra at the points labeled in Fig. 3(a) corresponding to a boron particle (A), an iron rich grain (B) and a niobium rich one (C). Figure 3(d) shows the evolution of the average powder particle size and figure 3(e) the most probable Fe content in a powder particle as a function of the equivalent milling time, which is indicative of the degree of homogenization as it must tend to the nominal value marked by a horizontal line.

JOM, 65 (2013) 870-882
http://dx.doi.org/10.1007/s11837-013-0616-1

The average size of powder particles, <*d*>, can initially increase when starting from small enough micrometric powder. At this stage the powder is still not work hardened and cold welding phenomena dominate over fracture. This implies that the starting size of the powders have no significant effect on the final size achieved after ball milling. Once powder is hard worked enough and this maximum size is achieved, fracture of particles is prevailing over cold welding mechanism and the average size reduces to a saturation value. Average particle size is affected by temperature (as temperature increases in the vial, welding of particles is enhanced over fracturing). Therefore, representation of <*d*> values, obtained at different Ω, as a function of an equivalent time can deviate from a single line when high values of Ω are considered [12].

Homogenization is progressively achieved but even after long milling times, there is some dispersion in the composition around the average value [24]. Analytical techniques such as EDS also help to detect contamination from the milling media, e.g. Cr in Fe-based alloys, which appropriately rescales using the equivalent time [12]. Contamination from milling media needs to be taken into account in order to choose the right materials for vials and balls to minimize its effect.

3.2 Global microstructural characterization

Very relevant data are obtained using X-ray diffraction (XRD). This technique supplies information on the phases present in the powder and their relative fraction as well as on different parameters of these phases (crystal size, microstrains, lattice parameters). It is worth mentioning that light elements have a poor scattering factor and thus phases rich in light elements cannot be well described, especially when other phases are present. Starting from a mixture of pure powders, a general description of

JOM, 65 (2013) 870-882
http://dx.doi.org/10.1007/s11837-013-0616-1

this evolution of XRD patterns can be as follows. Initially, the different pure phases are distinguishable (except for light elements such as boron). The peaks become broader, as a consequence of crystal size reduction and microstrains increase, and they shift their angular position, indicating changes in the lattice parameter. With respect to Fe-based alloys, in which we focus this paper, generally a bcc α-Fe type supersaturated solid solution is formed and the peaks corresponding to the other phases progressively disappear. Finally, for certain compositions [2, 25], an amorphous phase can be produced after destabilization of the long range order of the bcc supersaturated solid solution. Figure 4 shows how XRD parameters rescale using the equivalent milling time. This indicates that the following approximation is correct: The degree of microstructural change is only dependent on the amount of energy transferred from the milling media to the powder.

3.3 Local microstructural characterization

Transmission electron microscopy (TEM) is a powerful technique to achieve information on the microstructure features at the crystallite scale. However, TEM sample production from magnetic powder presents some difficulties. When the powder is simply deposited onto a grid, the typical size of powder particle can be too large to be electron transparent and studies are limited to edges [26-28], very convenient for nanopowders [19, 29]. Moreover, magnetic material can be instable under the electron beam. Powder particles embedded on resin can be affected by preferenctial action when electropolishing or ion beam thinning. In some studies, powders were embedded in Al [30] or Ni [31] plates for posterior thinning using an ion beam. Most recently, a new procedure known as lift-out technique has been developed using focus ion beam (FIB) microscopes [32]. In this technique, a slice thin enough to be electron transparent is extracted from a single powder particle. The procedure is shown in figure 5(a-g). First a

powder particle is selected and the region of interest is protected by depositing a Pt layer. With the help of Ga ions beam, a thick slice is cut and welded to a micromanipulator (using Pt deposition), which takes this slice to be welded to a Cu grid. Once the sample is in its final position it is thinned down to less than 100 nm to be electron transparent. Thanks to this technique, wide regions with constant thickness can be obtained, which is very helpful for characterizing the nanocrystalline and/or amorphous microstructure. Some examples are shown in figure 5(h-j).

The good quality (i.e. constant thickness) of the TEM samples prepared by lift-out enables analytical studies such as EDS or EFTEM maps as shown in figure 6 and figure 7, respectively. The examples shown correspond to Fe-Nb-B and Fe-Nb-Ge systems, showing that whereas brittle boron remains forming inclusions even after long milling times [32, 33], brittle Ge crystals disappear after long milling and are totally incorporated to the Fe-matrix [34]. Cr contamination is also shown for Fe-Nb-B alloys milled using hardened steel vials and balls.

4. Magnetic properties

4.1 Hysteresis loops

As a general consequence of ball milling, the coercivities of amorphous and nanocrystalline powder particles are one order higher than those of similar compositions obtained by rapid quenching [23, 35, 36]. The main factors affecting this fact are the increase in magnetoelastic anisotropy due to increase of microstrains and the limitation in the mobility of domain walls due to the size of the powder particles. In fact, softening has been observed after annealing below crystallization [37, 38] (releasing microstrains) and after compaction of powders [39].

JOM, 65 (2013) 870-882
http://dx.doi.org/10.1007/s11837-013-0616-1

Figure 8(a-b) shows the trends followed by saturation magnetization, M_S, and coercivity, H_C, for different Fe-Nb-B samples. In the case of M_S, equivalent time approach is well followed [13]. However, H_C values can show some differences between samples milled at different frequencies [12], ascribed to the H_C dependence on the powder particle size, which is very sensitive to the temperature as commented above.

The evolution of the effective magnetic anisotropy ($K_{eff} = H_C M_S/p_C$; p_C=0.64 for cubic particles [40]) with milling time can be analyzed using two regimes: at short milling times, the increase in microstrains leads to an increase of the magnetoelastic anisotropy (linearly dependent on the internal stresses in the sample) and magnetic anisotropy increases; for long milling times, crystal size refinement leads to averaging out of magnetocrystalline anisotropy (a power dependence law with the crystal size) leading to a progressive reduction of K_{eff}.

Following the interpretation of Shen et al. [41], the total effective magnetic anisotropy of nanocrystalline powder samples can be obtained as the addition of three contributions: long-range magnetoelastic, $K_{\sigma,ma}$, ascribed to the powder particle size; and two average anisotropies ascribed to nanocrystal size, short range magnetoelastic, $\langle K_{\sigma,mi} \rangle$, and magnetocrystalline $\langle K_1 \rangle$.

$$K_{eff} = \sqrt{K_{\sigma,ma}^2 + \left\langle K_{\sigma,mi} \right\rangle^2 + \left\langle K_1 \right\rangle^2}$$

Which, considering the averaging at nanometric scale, leads to an implicit equation for K_{eff}.

$$K_{eff} = \sqrt{\left(\frac{3}{2}\lambda_S \sigma_{ma}\right)^2 + \left[\left(\frac{3}{2}\lambda_S \sigma_{mi}\right)^2 + K_1^2\right]\frac{D^3 K_{eff}^{3/2}}{A^{3/2}}}$$

JOM, 65 (2013) 870-882
http://dx.doi.org/10.1007/s11837-013-0616-1

where σ_{ma} and σ_{mi} are the macro and microstrain, respectively; λ_S is the saturation magnetostriction constant; K_1 is the magnetocrystalline anisotropy; D is the average crystal size; and A is the exchange stiffness constant (e.g. λ_S=-7 ppm, K_1~$2\cdot10^4$ J/m^3, A~10^{-11} J/m for α-Fe [42]).

This analysis can be extended to partially amorphous systems [43] as:

$$K_{eff} = \sqrt{\left(\frac{3}{2}\langle\lambda_S\rangle\sigma_{ma}\right)^2 + \left[\left(\frac{3}{2}\langle\lambda_S\rangle\sigma_{mi}\right)^2 + \left(X_C K_1\right)^2\right]\frac{D^3 K_{eff}^{3/2}}{A^{3/2}}}$$

where X_C is the crystalline fraction and λ_S has been substituted by an average value, which can be estimated as a first approximation as:

$$<\lambda> = X_C\lambda_S^{Cr} + (1 - X_C)\lambda_S^{Am} = \lambda_S^{Am} + X_C\left(\lambda_S^{Cr} - \lambda_S^{Am}\right)$$

where the superscripts *Cr* and *Am* in λ_S refer to the magnetostriction values of the crystalline and amorphous phases, respectively. If both magnetostrictions are similar, the dependence with the crystalline fraction can be neglected.

Figure 8(c) shows the evolution of K_{eff} for short milling times as a function of microstrain and figure 8(d) shows a plot of K_{eff}^2 vs. $X_C^2D^3K_{eff}^{3/2}$ for long milling times. As microstrain is proportional to the square root of the dislocation density, a linear dependence of K_{eff} with microstrains is in agreement with the interpretation of Shen et al. [41]. For long milling times, the model allows us to obtain some information about the exchange stiffness and/or the magnetocrystalline anisotropy constant.

4.2 Magnetocaloric effect

Magnetocaloric effect (MCE) has been studied for several ball milled Fe-based amorphous and nanocrystalline alloys [44-54]. In order to do so, Maxwell equation is

JOM, 65 (2013) 870-882
http://dx.doi.org/10.1007/s11837-013-0616-1

widely used to obtain the isothermal magnetic entropy change around the second order phase transition corresponding to the ferro-paramagnetic change of the amorphous phase:

$$\Delta S_M(T) = \int_{H_0}^{H_{MAX}} \left(\frac{dM}{dT}\right)_H dH$$

Calculated for a field change from H_0 to H_{MAX} at a temperature T. Generally, H_0=0 T and MCE is referred to the ΔH value.

Figure 9(a) shows $\Delta S_M(T)$ curves for several partially amorphous compositions as a function of the crystalline fraction for a field change of 1.5 T. Peak values of $\Delta S_M(T)$ and refrigerant capacity estimated as the product of that value for the full width at half maximum of the peak are shown as a function of the crystalline fraction in figure 9(b-c). Generally, peak values are lower but the MCE curves are broader than for amorphous samples obtained by rapid quenching [55], leading to an enhancement of the refrigerant capacity. Also, as a general trend, MCE ascribed to the Curie temperature of the amorphous phase diminishes with the increase of crystalline fraction, due to the very different Curie temperatures of the amorphous and crystalline phases. However, in some cases, the presence of intermetallic phases with suitable Curie temperatures leads to an enhancement of the refrigerant capacity [49].

4.3 Mössbauer spectroscopy

^{57}Fe Mössbauer spectroscopy has been shown as a very useful tool in the study of the local environments of Fe atoms in Fe-base alloys, supplying relevant magnetic information. Three are the main parameters involved in Mössbauer analysis: isomer shift, quadrupole splitting and hyperfine magnetic field (HF) interaction, leading to a shift of the absorption line, a doublet and a sextet, respectively [56]. The combination of

these three factors will determine the number of lines and its asymmetry for each single Fe environment (usually restricted to the first two neighboring shells: near neighbors, NN, and next near neighbors, NNN).

Quadrupole splitting is ascribed to an asymmetric environment of the Fe atom, thus for metallic alloys a first approximation is to set this value to zero. This is especially significant in highly disordered systems were the number of possible Fe neighbourhoods are large and thus the number of fitting parameters increases, being necessary to use contributions described by distributions of hyperfine fields instead of a few discrete sites. Additionally, ambiguities arise for very low hyperfine field contributions (<5 T) in such complex systems, as they could also be represented by singlets or doublets: i.e. paramagnetic sites.

A single Mössbauer contribution (site) can describe a phase only having a single Fe environment. For example, pure α-Fe with Fe atoms surrounded by 8 Fe atoms as NN and 6 Fe atoms as NNN. When this does not occur, there should be recognized the different Fe sites in the phase. For example, considering the ordered α'-FeCo, for 1:1 stochiometry each Fe has 8 Co atoms as NN and 6 Fe atoms as NNN. However, α' phase exists in a certain compositional range and thus an excess of Fe from 1:1 stoichiometry should imply some Fe atoms in Co sites and thus, there will be Fe atoms surrounded by 8 Co atoms or 7 Co atoms plus 1 Fe atom or even 8 Fe atoms as NN, with certain probability depending on the composition. Therefore, up to 9 sextets (only considering NN) could be used (although probability decays with Fe atoms as NN). When the number of possible environments increases too much as in amorphous or nanocrystalline systems (due to interface contribution and variation of NN distances)

JOM, 65 (2013) 870-882
http://dx.doi.org/10.1007/s11837-013-0616-1

and supersaturated solid solutions, hyperfine field distributions are used for ferromagnetic samples, linking the *HF* and *IS* values linearly.

Figure 10(a) shows an example of the evolution of Mössbauer spectra with milling when the amorphous phase formed is paramagnetic. In this case, central absorption lines are enhanced and amorphous phase fractions can be obtained from the area ratio of the very low field contributions (in this systems hardly distinguishable from zero field contributions) with respect to the total area. Figure 10(b) shows that this technique is more sensitive than XRD for detection of low amorphous fractions. It is worth mentioning that the area-ratio obtained from Mössbauer refers to the fraction of Fe atoms located in amorphous phase. In order to obtain the total atomic fraction in amorphous phase, composition of the phases must be known. Mössbauer results are well correlated with magnetization measurements via the average hyperfine field, as shown in figure 10(c).

5. Thermal stability

Powder obtained after milling is a metastable system and can transit to a more stable system after annealing. Therefore, information about the stability of the obtained powder is very desirable. Differential thermal analysis (DTA) and differential scanning calorimetry (DSC) are used to obtain such information. Figure 11 shows some examples of DSC of ball milled powder. As temperature increases several features can be observed.

About ~400 K, for almost any powder, except for those milled during very short times, there is a step in the signal which coincides with a mass loss registered by

thermogravimetry. This could be ascribed to some desorption phenomena of the powders.

A very broad exothermic peak is ascribed to relaxation phenomena (stresses, crystalline phase, etc.). In many cases, this peak almost dominates the complete scan and jeopardizes other effects.

In some cases and after milling times at the limit of formation of the supersaturated solid solution, endothermic processes can appear [14, 57, 58]. A suitable explanation for these processes should be pseudomelting of some intermetallic phases formed during milling at intermediate stages. The strong deformation of those crystallites might contribute to their instability as well as the high surface to volume ratio in elongated and heavily deformed crystals.

Finally crystallization and/or recrystallization phenomena occur. Comparison of the kinetic parameters of these processes (onset and peak temperatures, activation energies, etc.) with those of amorphous (or nanocrystalline) phases formed through other routes helps to discern the quality of the milling products: composition of the amorphous, homogeneity, etc. It is worth mentioning that pressure affects crystallization onset, shifting it to higher temperatures [59]. This should be considered when hot pressing is used to compact the powders in their final shape for applications.

6. Conclusions

Mechanical alloying has been shown as a very versatile and “one step” technique to produce nanocrystalline and amorphous metastable systems, including those compositions with interesting soft magnetic properties. The huge amount of

parameters affecting ball milling technique makes the comparison difficult between different experiments. In this respect, dynamical studies leading to understand the dependency of the power release to the powder during milling are very helpful.

In order to correlate microstructure and properties, characterization must consider the two length scales present in the powder: powder particle size and crystal size. Homogenization can be easily achieved at the micrometric scale and differences between different powder particles are small at long enough milling times. However, at nanometric scale, inclusions of brittle materials such as boron can remain and it must be taken into account that the composition of the matrix differs from the nominal one.

Soft magnetic properties of as-milled powder are initially mainly affected by increase of the internal stresses and for long enough milling times by long range magnetoelastic anisotropy and average short range magnetoelastic and magnetocrystalline anisotropies.

Magnetocaloric effect in ball milled powders shows smaller ΔS_M peak values but broader curves than counterpart samples obtained by rapid quenching. In boron-containing alloys, the progressive amorphization and slow incorporation of boron lead to a dependence of magnetocaloric properties with the crystalline fraction.

Finally, thermal analysis indicates a large amount of relaxation heat and, in partially amorphous alloys, thermal stability of amorphous phase is in agreement with the values observed for similar amorphous phases obtained by rapid quenching.

7. Acknowledgements

JOM, 65 (2013) 870-882
http://dx.doi.org/10.1007/s11837-013-0616-1

Authors thank Prof. V. Franco for fruitful discussions and suggestions. This work was supported by the Spanish Ministry of Science and Innovation and EU FEDER (Project MAT 2010-20537), the PAI of the Regional Government of Andalucía (Project P10-FQM-6462), and the United States Office of Naval Research (Project N00014-11-1-0311). J.J. Ipus acknowledges a contract from the Regional Government of Andalucía.

JOM, 65 (2013) 870-882
http://dx.doi.org/10.1007/s11837-013-0616-1

Figure captions

Figure 1. Data obtained from Web of Science database. Results searching “mechanical alloy*” OR “ball mil*” as topic divided by results searching “material*” and normalized to the corresponding value in 1965.

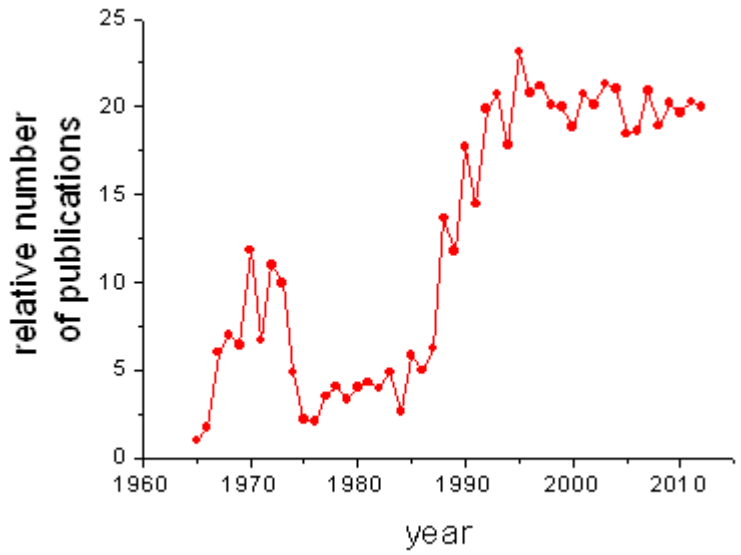

JOM, 65 (2013) 870-882
http://dx.doi.org/10.1007/s11837-013-0616-1

Figure 2. (a) P5 Fritsch mill and (b) trajectory followed by a single ball inside the vial. (c) P4 Fritsch Pulverisette mill and (d) trajectory followed by a single ball inside the vial. (e) Linear increase of the saturation temperature inside the vial during milling without powder using 50 steel balls in a 250 cm^3 GTMII system.

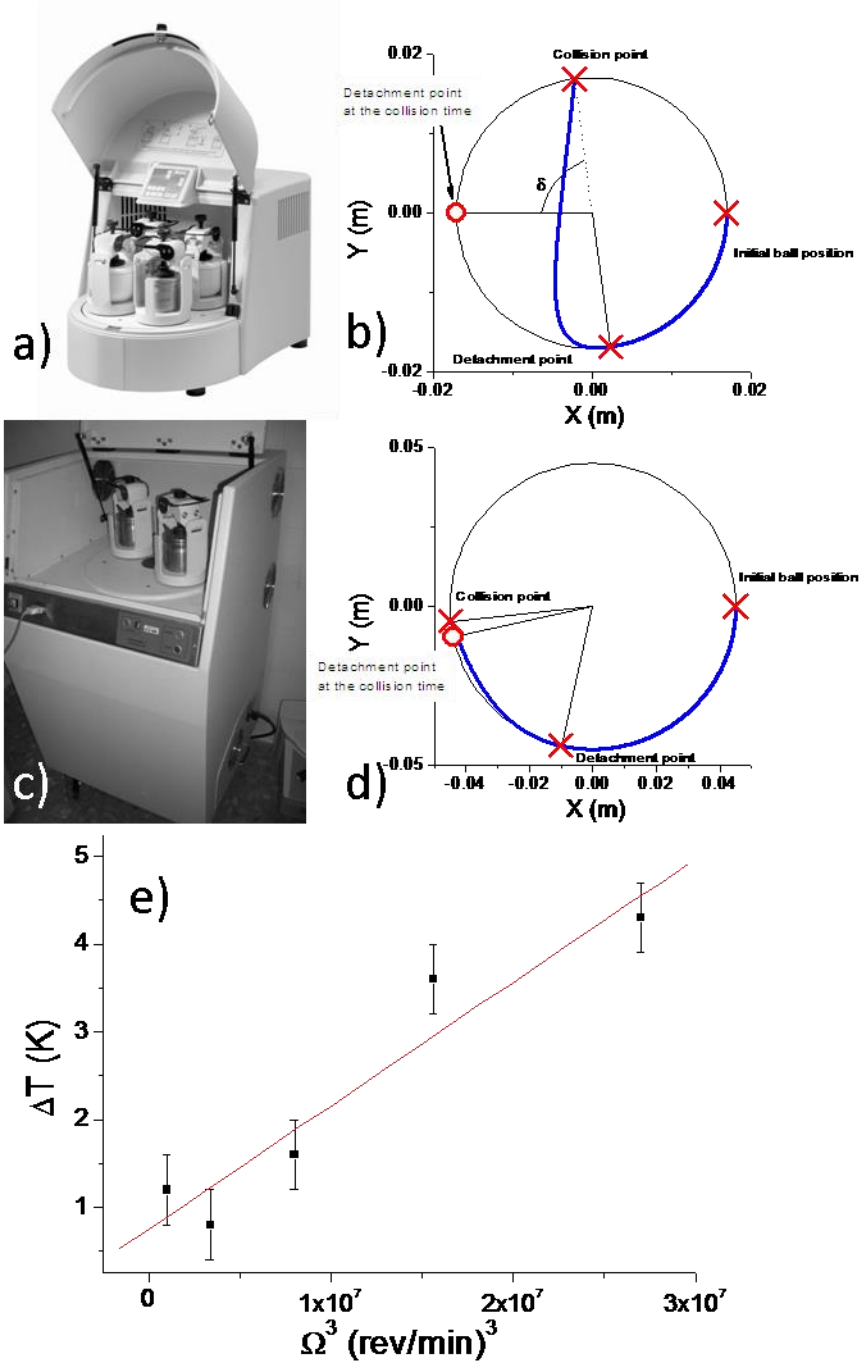

JOM, 65 (2013) 870-882
http://dx.doi.org/10.1007/s11837-013-0616-1

Figure 3. $Fe_{75}Nb_{10}B_{15}$ powder composition. (a) SEM SE and (b) BSE images of a powder particle after t_{eq}=2 h. (c) EDS spectra obtained from the regions marked in (a) as A, B and C. (d) Evolution of the average powder particle size and (e) most probable concentration of Fe in a powder particle as a function of the milling time (horizontal line indicates the nominal Fe composition).

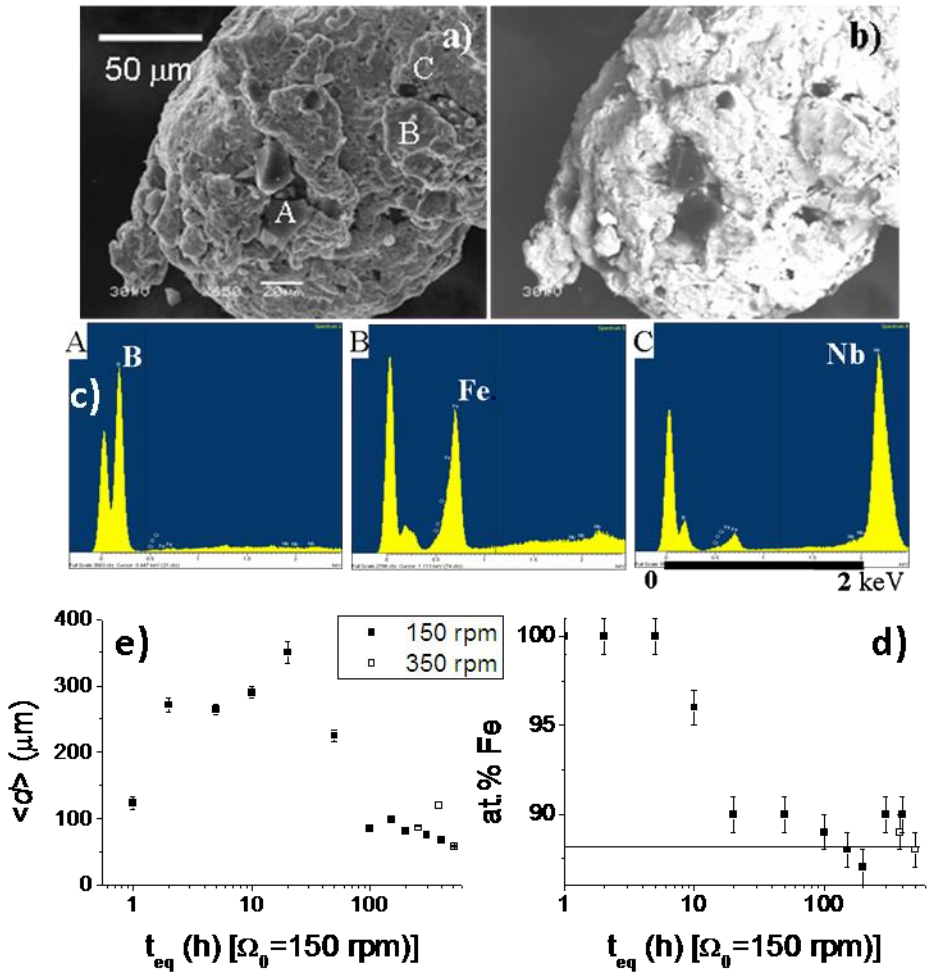

JOM, 65 (2013) 870-882
http://dx.doi.org/10.1007/s11837-013-0616-1

Figure 4. $(Fe_{1-x}Co_x)_{75}Nb_{10}B_{15}$ powder composition. (a) Evolution of XRD pattern for x=0.3, (b) lattice parameter and (c) crystalline fraction with equivalent milling time.

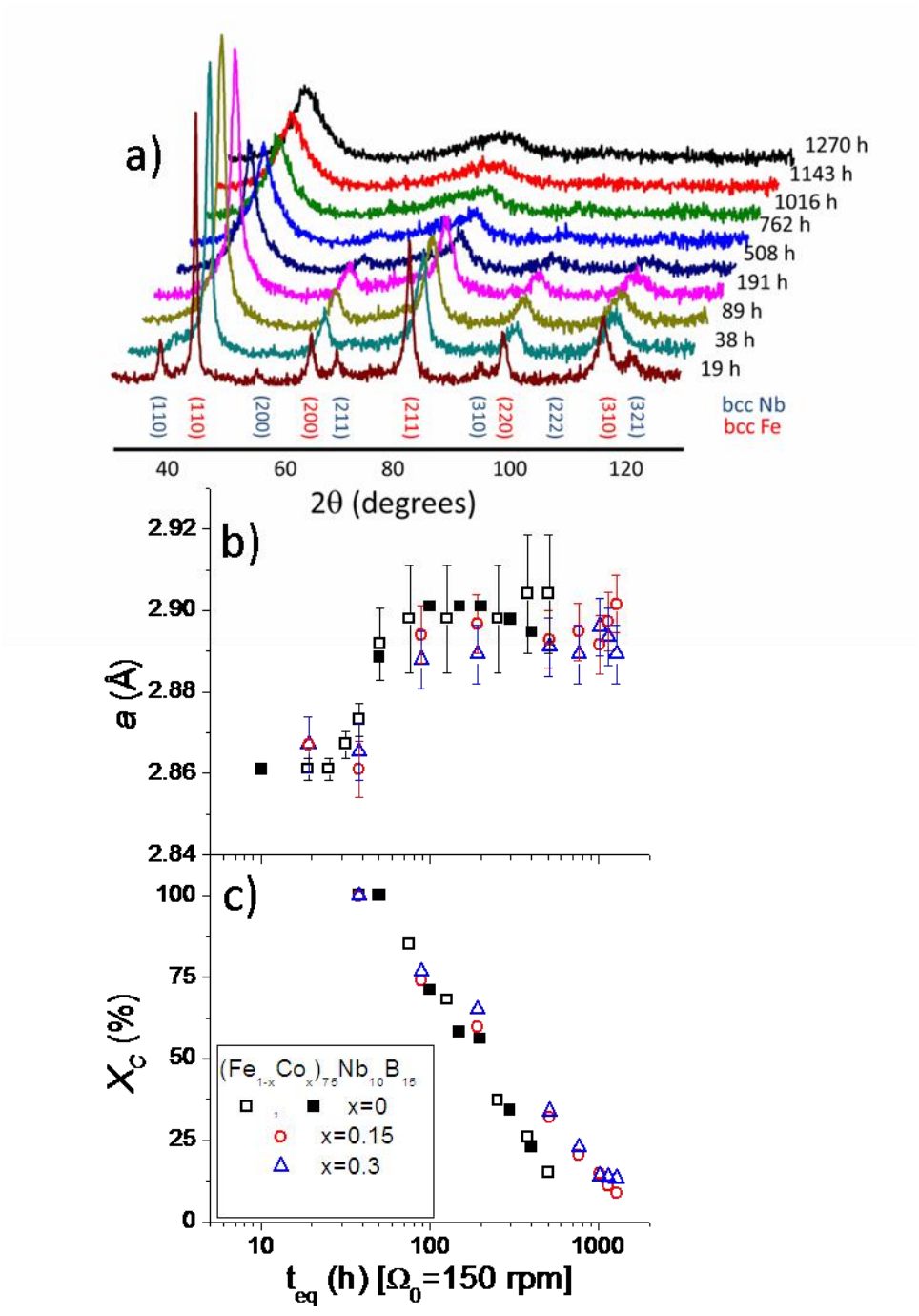

JOM, 65 (2013) 870-882
http://dx.doi.org/10.1007/s11837-013-0616-1

Figure 5. (a-g) FIB SE images of the different steps in lift out technique. (h) TEM BF image showing a general view of the TEM sample obtained. (i) TEM BF images of $Fe_{75}Nb_{10}B_{15}$ and (j) $Fe_{85}Nb_5B_{10}$ compositions after t_{eq}=400 h.

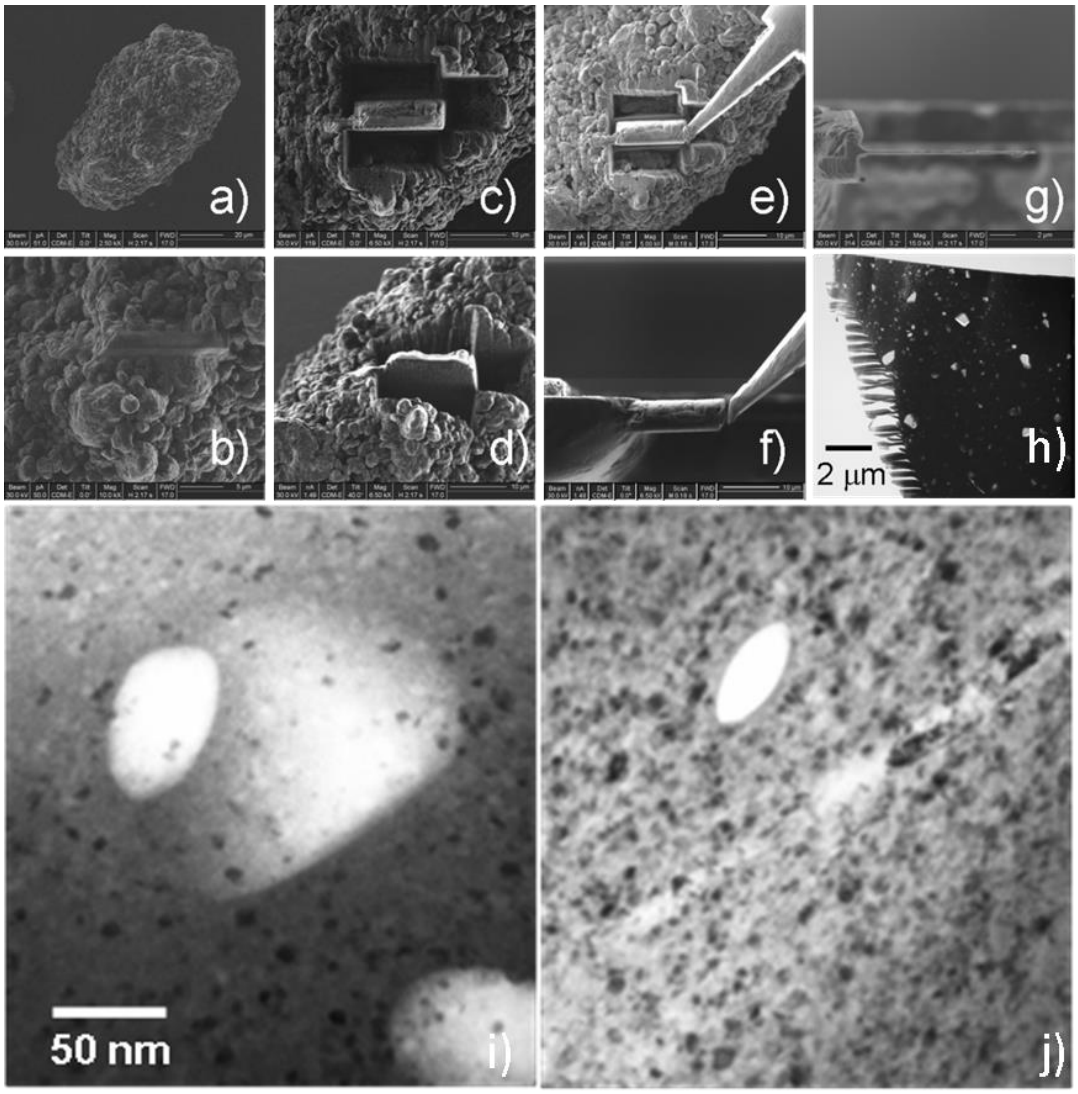

JOM, 65 (2013) 870-882
http://dx.doi.org/10.1007/s11837-013-0616-1

Figure 6. STEM DF images and EDS maps for (a) $Fe_{75}Nb_{10}B_{15}$ alloy after t_{eq}=50 h and (b) t_{eq}=400 h in a P4 mill, and (c) $Fe_{75}Nb_5Ge_{20}$ alloy t_{eq}=46 h in a P5 mill.

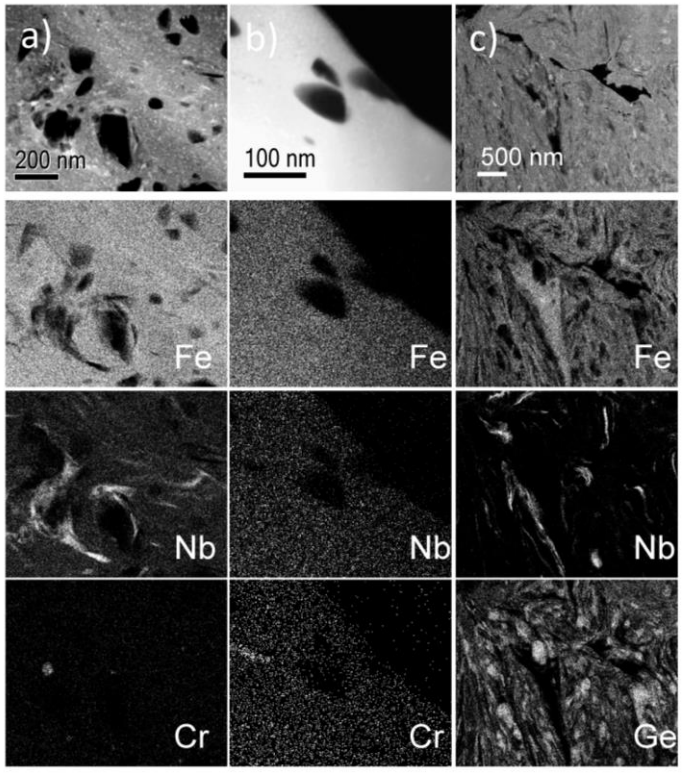

JOM, 65 (2013) 870-882
http://dx.doi.org/10.1007/s11837-013-0616-1

Figure 7. TEM BF images and EFTEM maps for (a) $Fe_{85}Nb_5B_{10}$ alloy after t_{eq}=400 h in a P4 mill, and (b) $Fe_{75}Nb_5Ge_{20}$ alloy t_{eq}=694 h in a P5 mill.

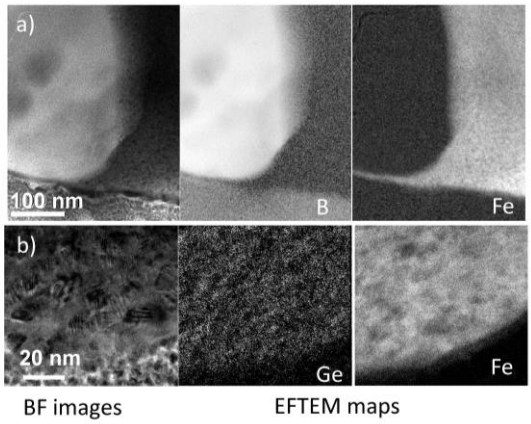

Figure 8. (a) Saturation magnetization and (b) coercivity as a function of t_{eq} for $Fe_{85}Nb_5B_{10}$ and $Fe_{75}Nb_{10}B_{15}$ alloys. Analysis of the effective magnetic anisotropy for short (c) and long (d) milling times.

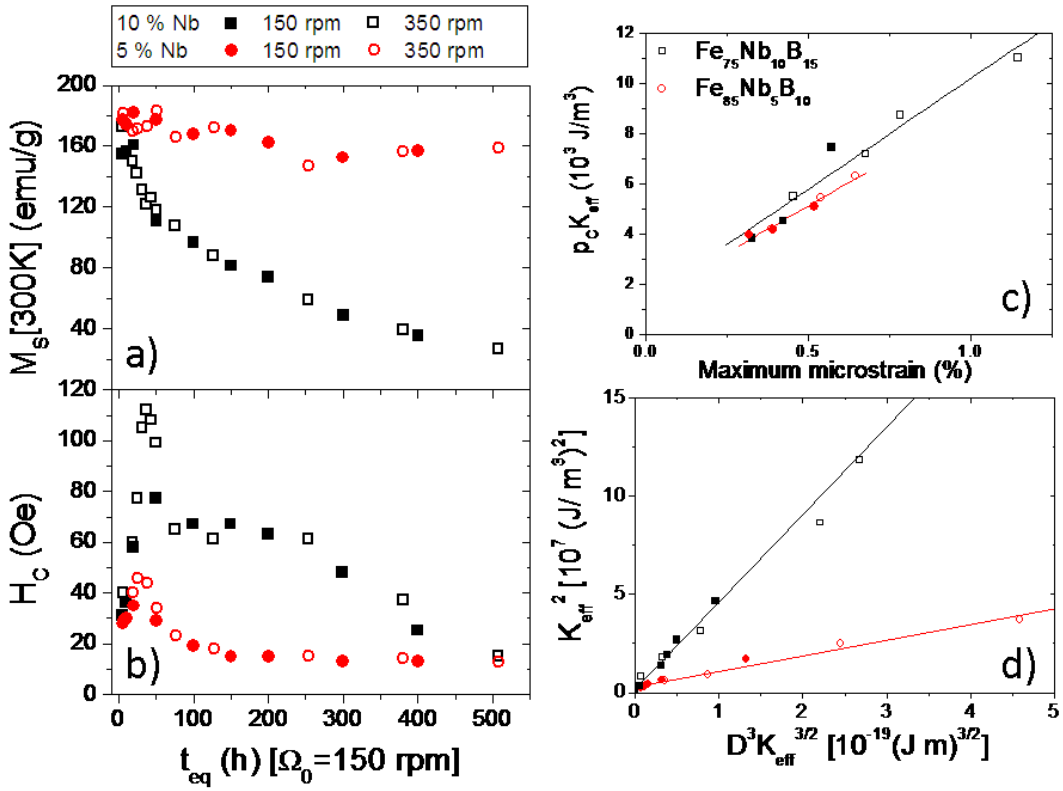

JOM, 65 (2013) 870-882
http://dx.doi.org/10.1007/s11837-013-0616-1

Figure 9. (a) $\Delta S_M(T)$ curves for ΔH=1.5 T as a function of the crystalline fraction for $(Fe_{1-x}Co_x)_{75}Nb_{10}B_{15}$ (x=0, 0.15, 0.3) alloys. (b) Peak values of ΔS_M and (c) RC_{FWHM}.

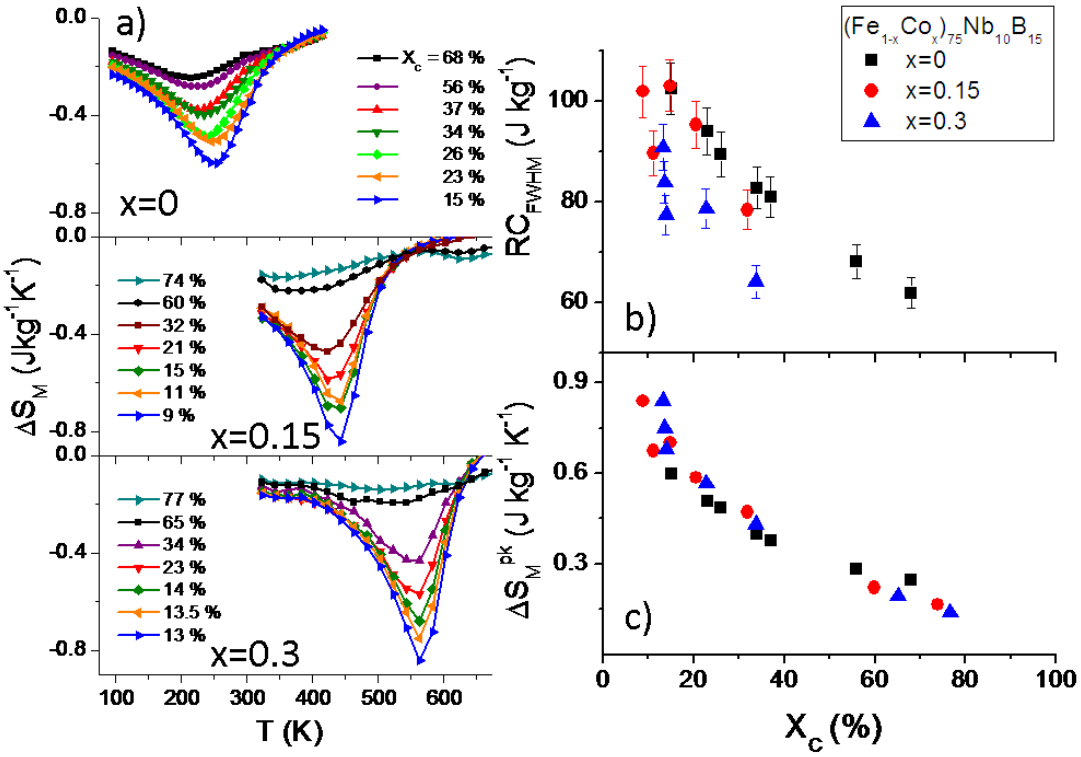

JOM, 65 (2013) 870-882
http://dx.doi.org/10.1007/s11837-013-0616-1

Figure 10. (a) Evolution of Mössbauer spectra with t_{eq}. (b) Correlation of the area fraction of low hyperfine fields contributions and crystalline fractions obtained from XRD. (c) linear correlation of average hyperfine field and saturation magnetization.

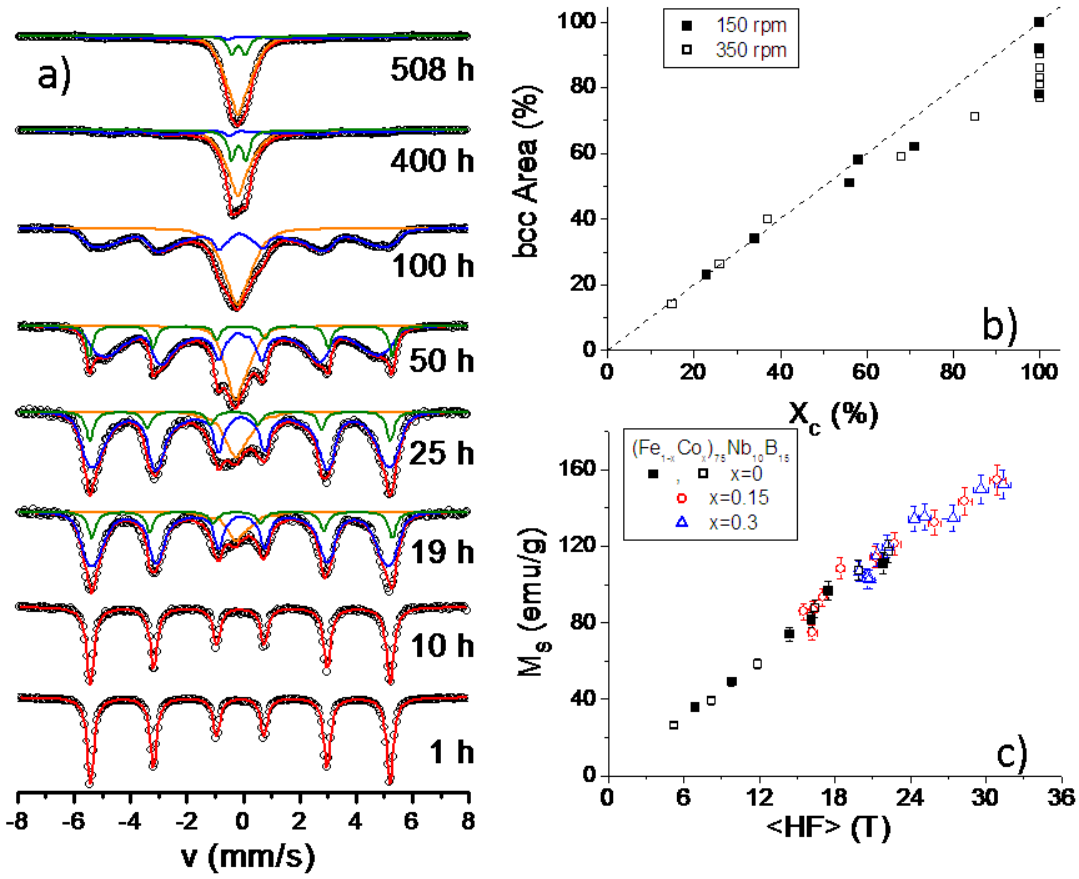

Figure 11. DSC scans for $Fe_{75}Nb_{10}B_{15}$ alloy after t_{eq}=5 and 508 h (crystallization peak at ~875 K), and for $Fe_{75}Nb_5Ge_{20}$ alloy (endothermic peak at ~725 K).

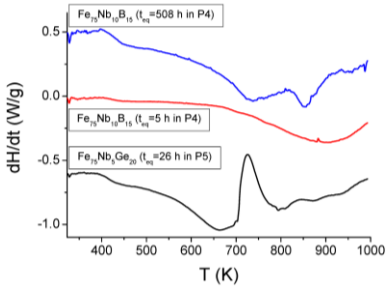

JOM, 65 (2013) 870-882
http://dx.doi.org/10.1007/s11837-013-0616-1

References

[1] J. S. Benjamin, T. E. Volin. Metal. Trans. 1974, vol. 5, pp. 1929-34.

[2] C. Suryanarayana, Prog. Materials Science. 2001, vol. 46, pp. 1-184.

[3] A. Y. Yermakov, Y. Y. Yurchikov, V. A. Barinov. Fiz. Metal. Metal. 1981, vol. 52, pp. 1184-93.

[4] C. C. Koch, O. B. Cavin, C. G. McKamey, J. O. Scarbrough. Appl. Phys. Lett. 1983, vol. 43, pp. 1017-9.

[5] M. E. McHenry, M. A. Willard, D. E. Laughlin. Prog. Mat. Sci. 1999, vol. 44, pp. 291-433.

[6] A. Inoue. Prog. Mat. Sci. 1998, vol. 43, pp. 365-520.

[7] F. Delogu, M. Monagheddu, G. Mulas, L. Schiffini, G. Cocco. Inter. J. Non-Eq. Process. 2000, vol. 11, pp. 235-69.

[8] F. Delogu, G. Mulas, L. Schiffini, G. Cocco. Mater. Sci. Eng. A. 2004, vol. 382, pp. 280-7.

[9] L. Takacs. Nanocrystalline materials by mechanical alloying and their magnetic properties in: "Processing and Properties of Nanocrystalline Materials," eds. C. Suryanarayana, J. Singh, and F. H. Froes, The Minerals, Metals & Materials Society, Warrendale, PA, 1996, pp. 453-464.

[10] A. Concas, N. Lai, M. Pisu, G. Cao. Chem. Eng. Sci. 2006, vol. 61, pp. 3746-60.

[11] M. Abdellaoui, E. Gaffet. Acta Metal. Mater. 1995, vol. 43, pp. 1087-98.

[12] J. J. Ipus, J. S. Blázquez, V. Franco, M. Millán, A. Conde, D. Oleszak, T. Kulik. Intermetallics. 2008, vol. 16, pp. 470-8.

[13] J. J. Ipus, J. S. Blázquez, V. Franco, A. Conde, L. F. Kiss. Intermetallics. 2010, vol. 18, pp. 565-8.

[14] J. S. Blázquez, J. J. Ipus, C. F. Conde, A. Conde. J. All. Compd. 2012, vol. 536, pp. S9-S12.

[15] C. C. Koch, J. D. Whittenberger. Intermetallics. 1996, vol. 4, pp. 339-55.

[16] C. C. Koch. Mater. Trans. JIM. 1995, vol. 36, pp. 85-95.

[17] E. M. Kirkpatrick, S. A. Majetich, M. E. McHenry. IEEE Trans. Mag. 1996, vol. 32, pp. 4502-4.

[18] V. M. Chakka, B. Altuncevahir, Z. Q. Jin, Y. Li, J. P. Liu. J. Appl. Phys. 2006, vol. 99, 08E912.

[19] B. Z. Cui, L. Y. Zheng, W. F. Li, J. F. Liu, G. C. Hadjipanayis. Acta Mater. 2012, vol. 60, pp. 1721-30.

[20] N. G. Akdogan, W. F. Li, G. C. Hadjipanayis. J. Nanoparticle Res. 2012, vol. 14.

[21] J. Bednarcik, K. Saksl, R. Nicula, S. Roth, H. Franz. J. Non-Crys. Sol. 2008, vol. 354, pp. 5117-9.

[22] K. J. Miller, A. Colletti, P. J. Papi, M. E. McHenry. J. Appl. Phys. 2010, vol. 107, 09A313.

[23] J. J. Ipus, J. S. Blázquez, V. Franco, A. Conde. Intermetallics. 2007, vol. 15, pp. 1132-8.

[24] J. J. Ipus, J. S. Blázquez, V. Franco, A. Conde. Intermetallics. 2008, vol. 16, pp. 1073-82.

[25] L. Schultz. Mat. Sci. Eng. 1988, vol. 97, pp. 15-23.

[26] K. J. Miller, M. Sofman, K. McNerny, M. E. McHenry. J. Appl. Phys. 2010, vol. 107, 09A305.

[27] Y. P. Shen, H. H. Hng, J. T. Oh. J. All. Compd. 2004, vol. 379, pp. 266-71.

[28] A. H. Taghvaei, M. Stoica, G. Vaughan, M. Ghaffari, S. Maleksaeedi, K. Janghorban. J. All. Compd. 2012, vol. 512, pp. 85-93.

[29] K. Simeonidis, C. Sarafidis, E. Papastergiadis, M. Angelakeris, I. Tsiaoussis, O. Kalogirou. Intermetallics. 2011, vol. 19, pp. 589-95.

[30] M. Krasnowski, H. Matyja. Mater. Sci. Forum. 2000, vol. 343-346, pp. 302-7.

[31] Y. J. Liu, I. T. H. Chang. Mat. Sci. Eng. A. 2002, vol. 325, pp. 25-30.

[32] J. J. Ipus, J. S. Blázquez, S. Lozano-Perez, A. Conde. Phil. Mag. 2009, vol. 89, pp. 1415-23.

[33] S. Katakam, J. Y. Hwang, H. Vora, S. P. Harimkar, R. Banerjee, N. B. Dahotre. Scripta Mater. 2012, vol. 66, pp. 538-41.

[34] J. J. Ipus, J. S. Blazquez, A. Conde, S. Lozano-Perez. J. All. Compd. 2010, vol. 505, pp. 86-90.

[35] N. Schlorke, J. Eckert, L. Schultz. J. Phys. D-Appl. Phys. 1999, vol. 32, pp. 855-61.

[36] J. J. Ipus, J. S. Blázquez, V. Franco, C. F. Conde, A. Conde. J. All. Compd. 2011, vol. 509, pp. 1407-10.

[37] S. Roth, M. Stoica, J. Degmova, U. Gaitzsch, J. Eckert, L. Schultz. J. Mag. Mag. Mat. 2006, vol. 304, pp. 192-6.

[38] K. Gheisari, S. Shahriari, S. Javadpour. J. All. Compd. 2013, vol. 552, pp. 146-51.

[39] M. H. Stoica, J. Degmova, S. Roth, J. Eckert, H. Grahl, L. Schultz, A. R. Yavari, A. Kvick, G. Heunen. 2002, vol. 43, pp. 1966-73.

[40] G. Herzer. IEEE Trans. Mag. 1990, vol. 26, pp. 1397-402.

[41] T. Shen, R. Schwarz, J. Thompson. Phys. Rev. B. 2005, vol. 72.

[42] R. C. O'Handley. Modern Magnetic Materials. Principles and Applications (Wiley, New York, 2000). 2000.

[43] J. J. Ipus, J. S. Blázquez, V. Franco, A. Conde, S. Lozano-Perez. Analysis of the magnetic anisotropy in Fe-Co-Nb-B alloys partially amorphized by mechanical alloying. Physics Express. 2012, vol. 2, pp. 1-7.

[44] H. Ucar, J. J. Ipus, V. Franco, M. E. McHenry, D. E. Laughlin. JOM. 2012, vol. 64, pp. 782-8.

[45] J. J. Ipus, J. S. Blázquez, V. Franco, A. Conde, L. F. Kiss. J. Appl. Phys. 2009, vol. 105, pp. 123922.

[46] J. J. Ipus, J. S. Blázquez, V. Franco, A. Conde. J. All. Compd. 2010, vol. 496, pp. 7-12.

[47] J. J. Ipus, H. Ucar, M. E. McHenry. IEEE Trans. Mag. 2011, vol. 47, pp. 2494-7.

[48] N. J. Jones, H. Ucar, J. J. Ipus, M. E. McHenry, D. E. Laughlin. J. Appl. Phys. 2012, vol. 111.

[49] J. S. Blazquez, V. Franco, A. Conde. Intermetallics. 2012, vol. 26, pp. 52-6.

[50] A. Chrobak, A. Bajorek, G. Chelkowska, G. Haneczok, M. Kwiecien. Phys. Stat. Solidi a. 2009, vol. 206, pp. 731-7.

[51] J. Gass, H. Srikanth, N. Kislov, S. S. Srinivasan, Y. Emirov. J. Appl. Phys. 2008, vol. 103.

[52] P. Gorria, P. Alvarez, J. Sanchez Marcos, J. L. Sanchez Llamazares, M. J. Perez, J. A. Blanco. Acta Mater. 2009, vol. 57, pp. 1724-33.

[53] K. Mandal, D. Pal, O. Gutfleisch, P. Kerschl, K. H. Mueller. J. Appl. Phys. 2007, vol. 102.

[54] D. M. Rajkuma, M. M. Raja, R. Gopalan, V. Chandrasekaran. J. Mag. Mag. Mater. 2008, vol. 320, pp. 1479-84.

[55] V. Franco, J. S. Blázquez, B. Ingale, A. Conde. Annual Rev. Mater. Res. 2012, vol 422012. p. 305-42.

[56] P. Gutlich, E. Bill, A. X. Trautwein. Mössbauer Spectroscopy and Transition Metal Chemistry. Fundamentals and Applications. Springer, Heidelberg, (2011).

[57] J. S. Blázquez, J. J. Ipus, M. Millán, V. Franco, A. Conde, D. Oleszak, T. Kulik. J. All. Compd. 2009, vol. 469, pp. 169-78.

[58] J. He, F. Zhou, G. Chang, E. J. Lavernia. J. Mater. Sci. 2001, vol. 36, pp. 2955-64.

[59] J. J. Ipus, J. S. Blázquez, V. Franco, A. Conde, M. Krasnowski, T. Kulik, L. F. Kiss. J. Appl. Phys. 2010, vol. 107, 073901.